Sensitivity of PAZ LEO Polarimetric GNSS Radio-Occultation Experiment to Precipitation Events

Estel Cardellach, *Member, IEEE*, Sergio Tomás, Santi Oliveras, Ramon Padullés, Antonio Rius, *Member, IEEE*, Manuel de la Torre-Juárez, Francis Joseph Turk, Chi O. Ao, E. Robert Kursinski, Bill Schreiner, Dave Ector, and Lídia Cucurull

***Abstract*—A Global Navigation Satellite System (GNSS) radio occultation (RO) experiment is being accommodated in the Spanish low Earth orbiter for Earth Observation PAZ. The RO payload will provide globally distributed vertical thermodynamic profiles of the atmosphere suitable to be assimilated into weather numerical prediction models. The Ground Segment services of the U.S. National Oceanographic and Atmospheric Administration and standard-RO processing services by University Corporation for Atmospheric Research (USA) will be available under best effort basis. Moreover, the mission will run, for the first time, a double-polarization GNSS RO experiment to assess the capabilities of polarimetric GNSS RO for sensing heavy rain events. This paper introduces the Radio-Occultation and Heavy Precipitation experiment aboard PAZ and performs a theoretical analysis of the concept. The L-band GNSS polarimetric observables to be used during the experiment are presented, and their sensitivity to moderate to heavy precipitation events is evaluated. This study shows that intense rain events will induce polarimetric features above the detectability level.**

***Index Terms*—Global Navigation Satellite System (GNSS) radio occultation (RO), heavy rain, remote sensing precipitation.**

Manuscript received August 28, 2013; revised February 10, 2014; accepted April 11, 2014. These studies are supported in part by the Spanish Ministry of Economy and Competitiveness (AYA2011-29183-C02-02, ACI2010-1089, and ACI2009-1023) and in part by NASA Grants (ROSES 10-GEOIM10-0018 and ROSES NNH10ZDA001N). E. Cardellach is under the Spanish *Ramón y Cajal* Programme. Some of these grants are partially supported by Fondo Europeo de Desarrollo Regional (FEDER) Funds. The Radio-Occultation and Heavy Precipitation with PAZ experiment has only been possible under a Consejo Superior de Investigaciones Científicas (CSIC)-HISDESAT agreement, while some of its ground segment services were possible owing to agreements between Institute of Space Sciences (ICE)-National Oceanographic and Atmospheric Administration and ICE-University Corporation for Atmospheric Research. Authors M. de la Torre-Juárez, F. J. Turk, and C. O. Ao. performed this work at the Jet Propulsion Laboratory, California Institute of Technology, under a contract with the National Aeronautics and Space Administration (NASA). They were supported by NASA's programs for Applications of Geodetic Imaging, NNH10ZDA001N-GEOIM, and Advanced Concepts in Space Geodesy, NNH10ZDA001N-GEODESY.

E. Cardellach, S. Tomás, S. Oliveras, R. Padullés, and A. Rius are with the Institute of Space Sciences-Consejo Superior de Investigaciones Científicas (ICE-CSIC/Institut d'Estudis Espacials de Catalunya), 08193 Barcelona, Spain (e-mail: estel@ieec.uab.es).

M. de la Torre-Juárez, F. J. Turk, and C. O. Ao are with the Jet Propulsion Laboratory, California Institute of Technology, Pasadena, CA 91109 USA.

E. R. Kursinski is with Broadreach Engineering, CO 80401 USA.

B. Schreiner and D. Ector are with the University Corporation for Atmospheric Research, Boulder, CO 80401 USA.

L. Cucurull is with National Oceanic and Atmospheric Administration, Boulder, CO 80307-3000 USA.

Color versions of one or more of the figures in this paper are available online at http://ieeexplore.ieee.org.

Digital Object Identifier 10.1109/TGRS.2014.2320309

I. Introduction

THE Spanish Ministry for Science and Innovation (MICINN) approved in 2009 a proposal to include a polarimetric Global Navigation Satellite System (GNSS) radio occultation (RO) payload onboard the Spanish Earth Observation satellite PAZ. The PAZ mission, planned to be launched in 2014, was initially designed to carry a synthetic aperture radar (SAR) as primary and sole remote sensing payload. It included an IGOR+advanced Global Positioning System (GPS) receiver and corresponding antennas for precise orbit determination. The GPS is one of the GNSS constellations and the one being used by PAZ's Integrated GPS Occultation Receiver (IGOR). Because the technique discussed in this paper also applies to the rest of the GNSS constellations, both GNSS and GPS terms will be used indistinctly. After minor modifications, the design and software of the IGOR+GNSS receiver allows the tracking of occulting signals, i.e., signals transmitted by GNSS satellites setting below the horizon of the Earth (or rising above it). The RO technique originated in planetary sciences for the study of other planets' atmospheres and measures the delay and bending caused by the refractivity of the radio signals as they propagate. This delay can be used to obtain vertical radio-refractivity profiles and ionospheric total electron content. From radio refractivities, one can extract vertical profiles of thermodynamic variables, such as atmospheric pressure, temperature, and water vapor pressure, from the stratosphere down to the surface with a vertical resolution in the range of 100–300 m. We will call all these products *standard-RO* or thermodynamical products hereafter. RO thermodynamical profiles are assimilated operationally into several global numerical weather prediction (NWP) systems, e.g., [1]. Results at National Centers for Environmental Prediction (NCEP) show that ROs improve anomaly correlation scores by $\sim$8 h starting at day 4, which increases with extended forecast range [2]. It also helps in reducing model biases. European Centre for Medium-Range Weather Forecast (ECMWF) compared the impact of 24 operational observation systems, with the GNSS RO impact resulting among the top five [3]. The use of GNSS RO has been shown to significantly improve model forecast skill and is a key component of the operational observing system [4].

Missions currently providing this information in near real time (NRT) to the Numerical Weather Prediction Models (NWPM) are the constellation of six low Earth orbiters (LEOs)

(Taiwan/USA FORMOSAT-3/Constellation Observing System for Meteorology Ionosphere and Climate (COSMIC) mission), the EUMETSAT's GNSS Receiver for Atmospheric Sounding (GRAS) instruments aboard the METOP (A/B) satellites, and Gravity Recovery And Climate Experiment (GRACE) and TerraSAR-X LEOs, in the form of globally distributed profiles. However, the number of RO profiles risks to dramatically drop after the decommissioning of the COSMIC constellation. With a mission life expectancy of 5 years, the current yield of COSMIC is not ensured since 2012. PAZ is planned to be launched in 2014 which is before a new RO constellation is deployed: The first six LEOs of the operational COSMIC follow-on are planned to be launched in 2016. A few other LEOs are currently equipped with GNSS RO capabilities, but they are not providing their products in NRT for forecast applications. PAZ has thus potential to contribute by filling the gap of NRT RO data in the coming years.

The GNSS systems transmit right-hand circular-polarized (RHCP) signals, and as a consequence, all the RO missions and experiments deployed so far use RHCP receiving antennas. The main particularity and uniqueness of the PAZ RO mission is that the RHCP GNSS RO antenna has been replaced by a double polarization, H and V, antenna. These signals can be recombined to obtain the same standard thermodynamic profiles currently being generated with RHCP antennas. With polarimetric information in addition to the standard products, new applications can be envisaged from the additional information embedded in the polarimetric data. In particular, in the PAZ experiment, we seek to infer information on intense precipitation.

The GPS works at L-band (L1-GPS at 1.57542 GHz; L2-GPS at 1.22760 GHz). Although the frequencies of these signals were chosen such that they would suffer low attenuation by clouds or rain and enable all-weather operations, the depolarization effect induced by the flattening of the heavy precipitation drops may exceed some measurable threshold. Work done for the calibration and characterization of similar signals (Geostationary Operational Environmental Satellit (GOES) 11 L-band downlink at 1.5445-GHz RHCP) has found strong correlation between the depolarization ratio and heavy rain when measuring a downlink at a 14° elevation angle above the horizon [5]. The same concept, in backscattering geometry instead of forward-scattering, is used in polarimetric weather radars, working at 3 GHz (twice the L1-GPS). The depolarization effect increases as the propagation line aligns with the plane of the drops' flattening (nominally perpendicular to the local gravity, i.e., parallel to the local horizon). The RO signals cross the lower troposphere tangentially, i.e., along the local horizon, which should maximize the depolarization effect. The concept is sketched in Fig. 1.

We did not find scientific literature where the effects of precipitation into GNSS polarimetric observables have been analyzed. As stated in [5], the weather effects onto polarimetric propagation are generally unaddressed below 4 GHz. For these reasons, it is important to establish the expected theoretical sensitivity of polarimetric GNSS RO observables to precipitation events. The main goal of our study is thus to determine the detectability of heavy rain with polarimetric RO and to understand the mechanisms behind the concept as a secondary goal and first step toward designing the retrieval algorithms.

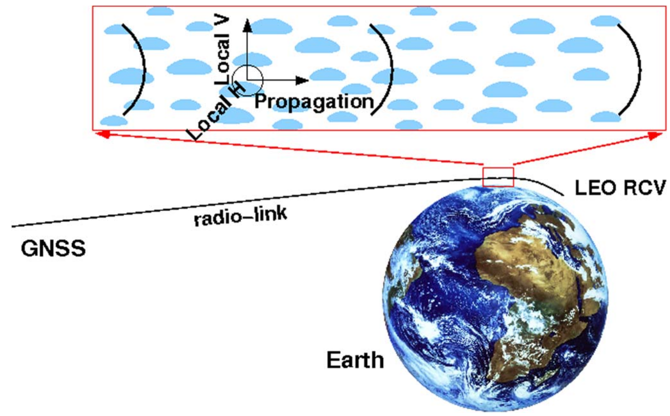

Fig. 1. Sketch of the ROHP measurement concept: At the lower troposphere, RHCP GNSS signals in RO radio link propagate tangentially, aligned with the plane of flatness of the rain drops (if no canting angle is accounted). In this situation, the depolarization effect is maximum. The receiver on board the PAZ mission will collect both polarization components.

Precipitation remains a poorly predicted event with current climate and weather model parametrization. A better understanding of the thermodynamics of heavy precipitation events is necessary toward improving climate models and quantifying the impact of climate variability on precipitation [6], [7]. The particular advantage of GNSS RO is that its signals are in the microwave spectrum which is influenced little by clouds. A few infrared sensors, such as the Atmospheric Infrared Sounder (AIRS), can profile atmospheric temperature/humidity with high vertical resolution but cannot penetrate through the optically thick clouds typically associated with precipitation [8]. Radar, microwave, and laser instruments such as Tropical Rainfall Measuring Mission (TRMM), Advanced Microwave Scanning Radiometer-Earth Observing System, and CloudSat measure the precipitation rates and even some physical drop properties but do not measure the water vapor nor the temperature profiles associated with these droplets. Polarimetric GNSS RO in the Radio-Occultation and Heavy Precipitation with PAZ (ROHP-PAZ) has thus the potential to be the only remote sensing technique to measure both precipitation rates and the coincident thermodynamic profiles.

The ROHP-PAZ experiment aims to be a proof of concept to exploit the potential capabilities of polarimetric RO toward detecting and quantifying heavy precipitation events. If successful, PAZ will open new applications of GNSS RO observations by providing coincident thermodynamic and precipitation information with high vertical resolution within regions covered by thick clouds. These measurements will overlap with those obtained by the Global Precipitation Measurement (GPM) mission, offering the potential for complementary observations.

After presenting the mission overview and RO payloads in Section II, the rest of this paper focuses on the polarimetric/precipitation experiment: Section III presents the GNSS polarimetric observables selected to maximize the precipitation information content, the forward scattering models are presented in Section IV, and a sensitivity study about the polarimetric response of these L-band observables

TABLE I
MEAN ORBITAL PARAMETERS

Mean semi-major axis:	6883.495 km
Mean eccentricity:	0.00107759
Mean inclination:	97.4219 deg

when crossing rain regions along the spaceborne RO geometry is shown in Sections V and VI.

II. PAZ RO MISSION

PAZ is owned and managed by HISDESAT, a mixed private/public company based in Spain. The Institute for Space Sciences (ICE) from the Spanish National Research Council (CSIC) is responsible for the RO experiment under collaborative agreements between HISDESAT and CSIC. Complementary agreements have also been signed between ICE-CSIC and the U.S. National Oceanographic and Atmospheric Administration (NOAA) and between ICE-CSIC and the University Corporation for Atmospheric Research (UCAR, USA) to contribute to the ground segment and processing chain of the RO component of the mission. These services will be provided under best effort basis. PAZ RO has been assigned the World Meteorological Organization (WMO) Binay Universal Form for the Representation of meteorological data (BUFR) code number 44 [9]. The products to be provided by UCAR, preferably in NRT, are not polarimetric, but recombined (equivalent to RHCP). The raw polarimetric data will be sent to ICE-CSIC/Institute d'Estudis Espacial de Catalunya (IEEC), from where the polarimetric and precipitation analysis will be developed. A dedicated data server at ICE-CSIC/IEEC will make the polarimetric data and precipitation products available to the scientific community.

The satellite launch is scheduled for 2014, from a Russian Dnepr vehicle, in a sun-synchronous nearly circular orbit at 514-km altitude (see further details of the orbit in Table I). The launch will be followed by a 6-month commissioning phase period and has an expected life of 7 years with a goal of 10 years.

The spacecraft, with ~1400-kg mass, has a hexagonal section of diameter of ~2.4 m and almost 5-m length (see artistic view in Fig. 2). The RO experiment is, in principle, absolutely decoupled from the satellite's main payload, an X-band SAR, except for sharing the GNSS receiver and complementary satellite health and attitude information. The SAR component of the mission requires precise orbit determination, achieved by means of an IGOR+GNSS receiver. This same receiver had been modified in other missions to track GNSS occulting signals through two ancillary channels [10], [11]. In these other RO missions, one of the ancillary channels tracks GNSS occulting signals as captured from a RO antenna located at the forward tip of the platform, pointing toward the limb of the Earth in the forward direction, while the other channel tracks the GNSS occulting signals as captured from another RO antenna at the posterior tip of the craft, pointing toward the limb of the Earth in the aft direction. The forward pointing channel is for rising occultations, whereas the aft pointing channel is for setting occultations.

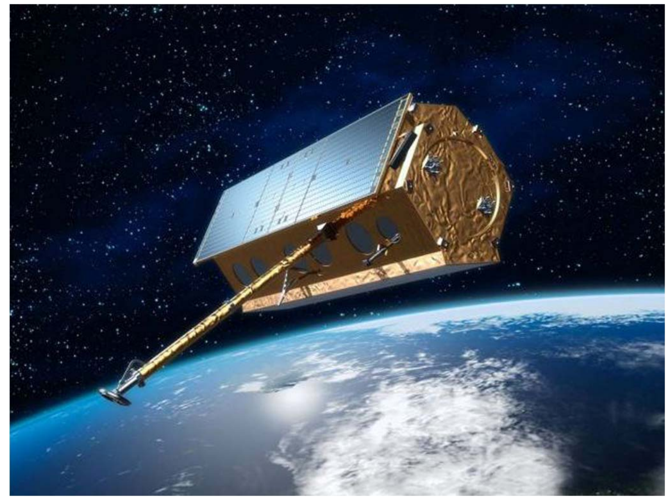

Fig. 2. Artistic view of PAZ satellite (courtesy of HISDESAT).

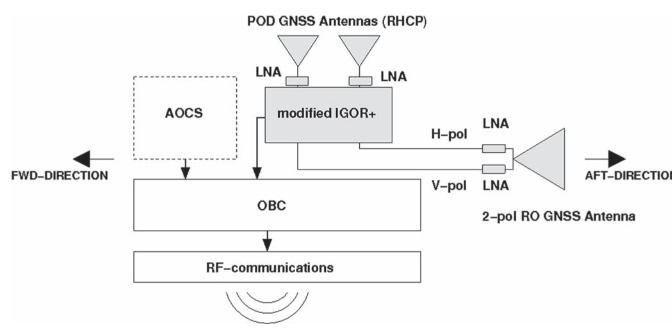

Fig. 3. Block diagram of the payload components involved in the RO data packages telemetered to the ground stations.

Similar modifications have been made in PAZ's IGOR receiver, except that both ancillary channels are connected to the setting (posterior) RO antenna. This RO antenna has two ports, at two linear polarizations. The RO channels of PAZ's IGOR will thus correspond to setting horizontal polarization (H-pol) and setting vertical polarization (V-pol) observations. They are configured to operate as master and slave channels, to guarantee that the same tracking parameters are used in both channels. The modes of operation are the same as in the former versions of the IGOR receiver (lock-loop and open-loop modes). No rising occultations will be gathered from PAZ. The RO data will be packed and downloaded to the RO ground stations (NOAA) together with ancillary information from the Attitude and Orbit Control Subsystem, as sketched in Figs. 3 and 4.

The RO antenna has been designed and manufactured by Haigh–Farr under contract with IGOR's manufacturing company, Broadreach Engineering. The design is based on the RO antennas aboard COSMIC and TerraSAR-X, customized to meet as much as possible the requirements of the ROHP experiment. The antenna is a five-element array, with a nominal gain of 13 dB at L1 (12.95-dB H-pol and 12.66-dB V-pol, as measured in an anechoic chamber) and 11.5 dB at L2 (11.67-dB H-pol and 11.12-dB V-pol). The cross-polar isolation at the Earth limb direction is around 27 dB at L1. The patterns around the limb of the Earth observation window are shown in Fig. 5.

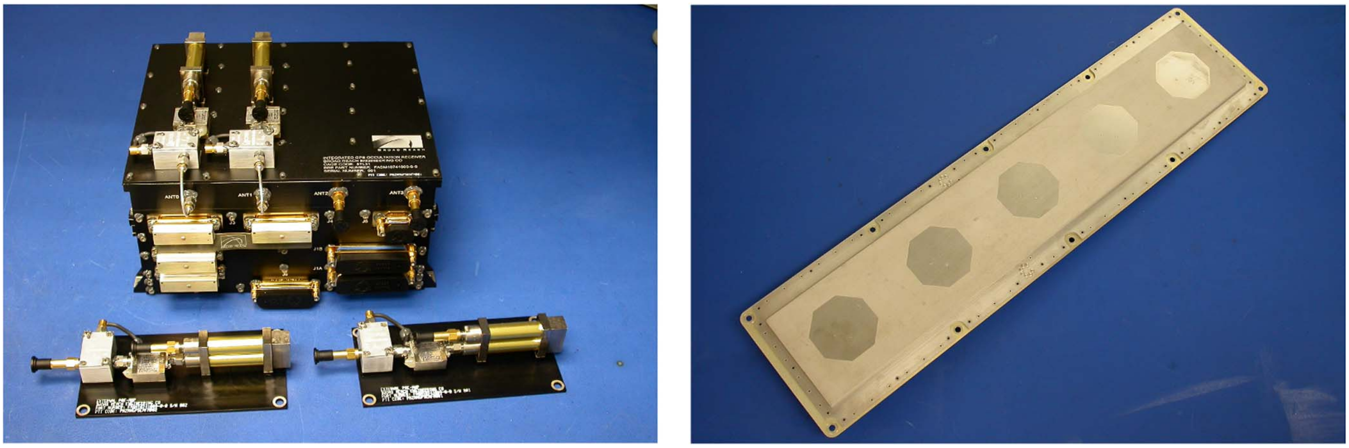

Fig. 4. (Left) PAZ's IGOR+flight unit and preamplifier assemblies for the POD (mounted directly on the receiver) and the RO antennas (mounted by the RO antennas). (Right) PAZ's dual-polarization RO antenna (flight unit).

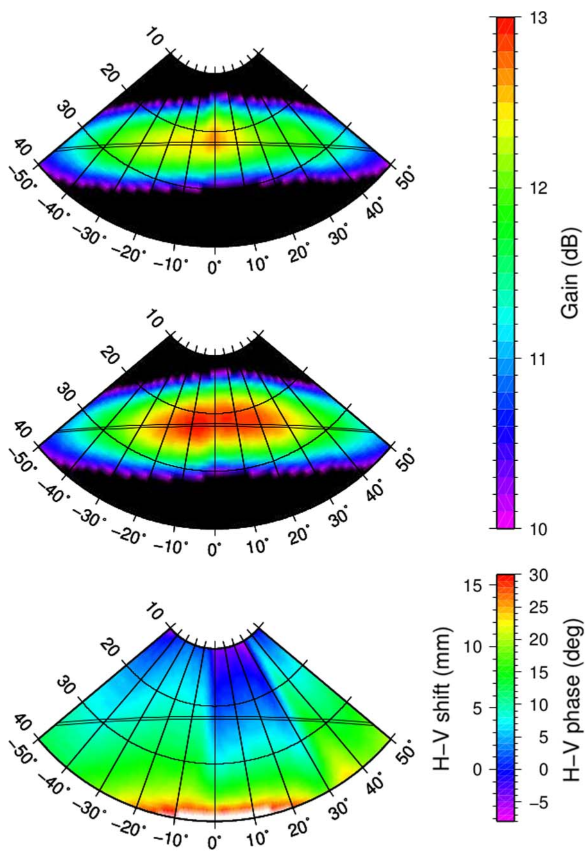

Fig. 5. PAZ RO antenna patterns measured at the anechoic chamber. The x- and y-axes correspond to the ϕ and θ angles of a spherical coordinate system with its z-axis pointing to the bore-sight of the antenna (antivelocity vector of the spacecraft). (Top) Gain at V-polarization. (Center) Gain at H-polarization. (Bottom) Phase difference between H and V patterns. The solid lines correspond to the limb of the Earth and a fixed atmospheric altitude of 20 km, where the rain occurs. No bending of the signal has been considered.

III. Selected Observables

The polarization ellipse of the electromagnetic field can be described by means of two angles. Using the notation found in [12], the Ψ angle can be obtained from the ratio between the amplitude of the field in two orthogonal linear projections (e.g., amplitudes of the horizontal and vertical polarization components in the PAZ RO antenna). The other angle that characterizes the ellipse of polarization is the phase shift Δ, obtained as the phase difference between both linear components at t_0. Purely circular polarization corresponds to $\Delta = \pm\pi/2$ rad. Both the ellipticity and orientation of the ellipse, as well as each of its axis lengths, are only functions of Ψ and Δ. As justified hereinafter, we suggest to deal with an observable related to Δ, i.e., to phase shifts rather than field amplitudes. In particular, we suggest to measure the departure of Δ with respect to the value that it would have if the received field were purely circular: $\Delta\phi = \Delta - \pi/2$. This observable relates to the depolarization induced by the birefringence of the rain drops, resulting in different phase velocities for different field orientations.

L-band signals penetrate through clouds and rain, experiencing little attenuation. However, it is also true that atmospheric media induce delays to the signals propagating through them, and under certain conditions, such delays might be different at different polarization states. GNSS signal structure and tracking algorithms are particularly suited to measure delays or ranges with great precision. The phase of the received signals is a very precise measure of changes in the range or delay between the transmitter and the receiver. Its precision depends on the received amplitude SNR as

$$\sigma_\phi = \frac{\lambda}{2\pi} \arctan\left(\frac{1}{\mathrm{SNR}}\right) (\mathrm{SNR} > 0) \tag{1}$$

(in units of delay length) where, for sufficiently high SNR values, $\arctan(1/\mathrm{SNR})$ can be approximated by $1/\mathrm{SNR}$. In order to determine the precision of the phase delay from GNSS RO links under precipitation conditions around the tangent point, COSMIC ROs have been collocated with precipitation measurements obtained with National Aeronautics and Space Administration (NASA)/Japan Aerospace eXploration Agency (JAXA) TRMM. Further details of the collocation process are detailed in Section V. The objective here is to establish a relationship between the SNR of the RO observations and the presence of rain along their radio links and to then apply (1) and determine the precision of the phase observables under different rain conditions. In principle, the gain of ROHP-PAZ's

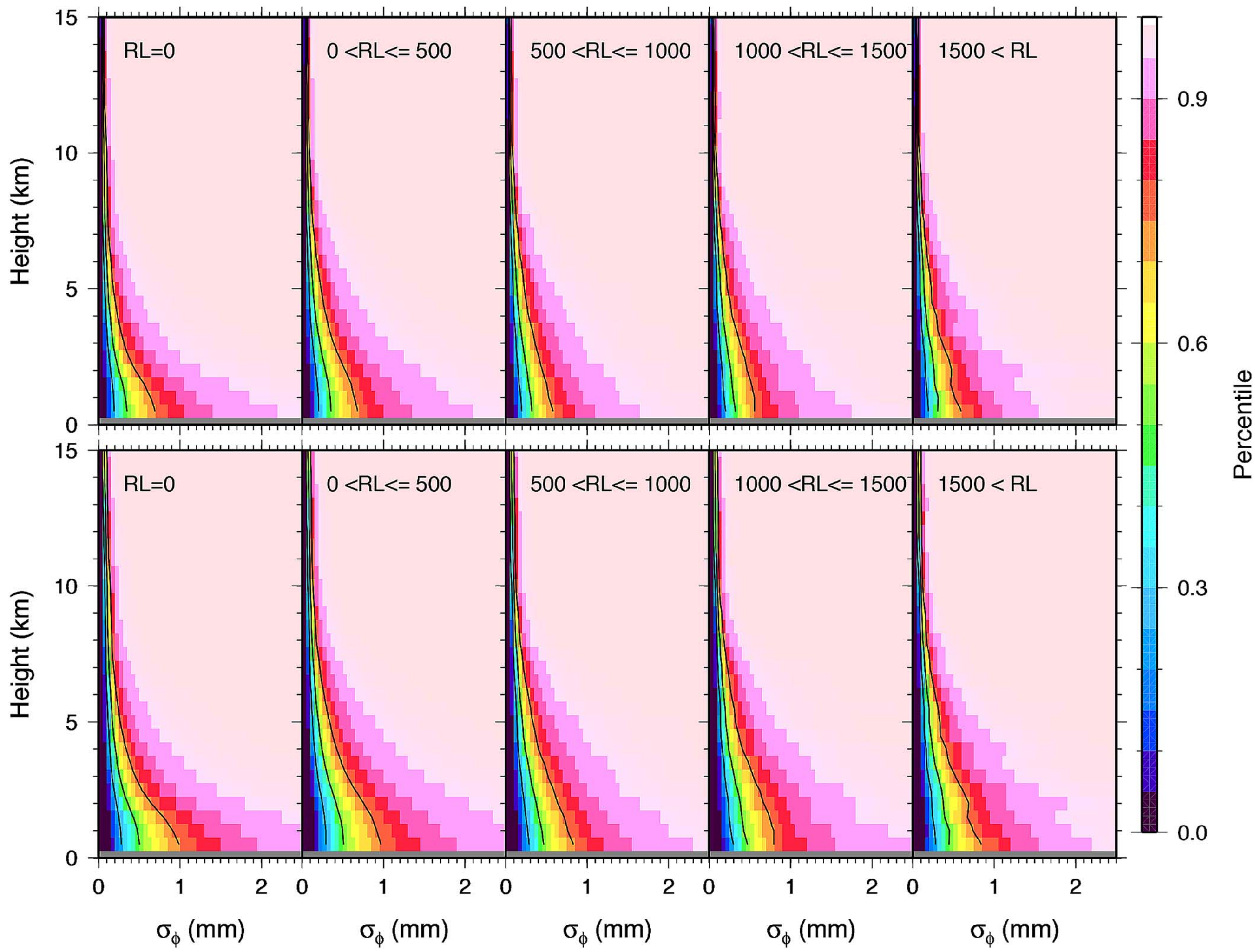

Fig. 6. (Top row) Percentile fraction of the precision of COSMIC's phase-delay measurements, σ_ϕ, as computed from real COSMIC 1-s SNR observations (more than 420 000 RO profiles) and (1). The percentile is computed at each altitude, in steps of 0.5 km, and defined as the fraction of events at that altitude with phase-delay precision equal or better than x. From left to right, different rain scenarios as determined from the collocation of COSMIC events with the TRMM mission, defined as the product between the mean rain rate (in mm/h) and the total rain length along the radio link (in km), $\langle R \rangle L$ (in mm/h km). The values of this product are grouped in five ranges: from (foremost left) rain-free to (foremost right) higher than 1500 in steps of 500 mm/h km (see histograms of these values in Fig. 7). This would correspond to PAZ's precision at each H or V port if its higher antenna gains could compensate the loss of half of the power (polarization mismatch) with respect to COSMIC. (Bottom) Same as top panel, but under a conservative assumption that PAZ's performance at each linear polarization port is worse than COSMIC RHCP measurements by -3 dB.

antenna should be slightly higher than COSMIC's. However, COSMIC's antennas are RHCP, matching the transmitted polarization features, whereas each of ROHP-PAZ's linear polarization antennas captures solely half of the power (polarimetric mismatch). As a consequence, we establish that PAZ performance at each antenna port (H/V) should be between 0 and -3 dB with respect to those on COSMIC.

The top row in Fig. 6 compiles the statistics of more than 420 000 COSMIC profiles which occurred in 2007, in terms of the precision of the phase observable, σ_ϕ, as a function of the altitude and precipitation. These precisions have been obtained from (1) and real SNR values of the COSMIC observations corresponding to 1-s observations. The statistics are separated according to different rain scenarios as deduced from the collocation against the TRMM precipitation mission. It is clear that the precision is little affected by various precipitation scenarios. At the lowest layers of the atmosphere, where precipitation occurs, 50% of the events present phase-delay precision level better or equal to 0.3 mm, 75% better or equal to 0.7 mm. This would correspond to the PAZ phase precision at each port (H or/and V) if its higher antenna gain with respect to COSMIC could fully compensate the polarization mismatch. If we consider a conservative -3-dB degradation of the SNR at each PAZ linear polarization port with respect to COSMIC RHCP performance, the resulting precision estimates are shown in the bottom row of Fig. 6. The 50 percentile of the precision per port is reduced to $\sigma_\phi \leq 0.5$ mm, and the 75 percentile is reduced to ≤ 1 mm, regardless of the amount of precipitation crossed by the radio link. Higher altitudes (where rain is still expected) present finer precision. The 75 percentiles at each altitude range are summarized in Table II. Histograms of the COSMIC events as a function of the rain scenario are presented in Fig. 7, which permit better comprehension of the statistics behind these values, the amount of cases within each scenario, and separate the distribution of rain rates with respect to the rain cell length.

TABLE II

EXPECTED PRECISION OF PAZ PHASE-DELAY OBSERVABLES, BASED ON 1-S SNR DATA OF MORE THAN 420 000 COSMIC RO EVENTS. VALUES EXTRACTED FROM 75-PERCENTILE LINES IN THE WORST CASES OF FIG. 6. THE TOP-FOUR ROWS OF THIS TABLE COMPILE THE PRECISION AT EACH PORT (H/V). THE BOTTOM-FOUR ROWS ESTIMATE THE PRECISION OF THE POLARIMETRIC PHASE-SHIFT OBSERVATION, $\Delta\phi$ IN (3), ASSUMING INDEPENDENT MEASUREMENTS AT EACH PORT. THE FIRST COLUMN ASSUMES THAT EACH PAZ ANTENNA LINEAR POLARIZED PORT WOULD PERFORM LIKE COSMIC RHCP. THE SECOND COLUMN ASSUMES THAT PAZ PERFORMANCE AT EACH PORT WOULD BE 3 dB WORSE THAN COSMIC RHCP. ACTUAL PAZ LINEAR POLARIZATION PERFORMANCES ARE EXPECTED TO BE IN BETWEEN THESE TWO ASSUMPTIONS

	COSMIC (mm)	**COSMIC-3dB (mm)**	**H (km)**
1-port σ_ϕ	0.1	0.15	≥10
	0.3	0.35	5-10
	0.6	0.8	2-5
	0.7	1	<2
Polarimetric $\sigma_{\boldsymbol{\Delta}\phi}$	0.1	0.2	≥10
	0.4	0.5	5-10
	0.9	1.1	2-5
	1	1.4	<2

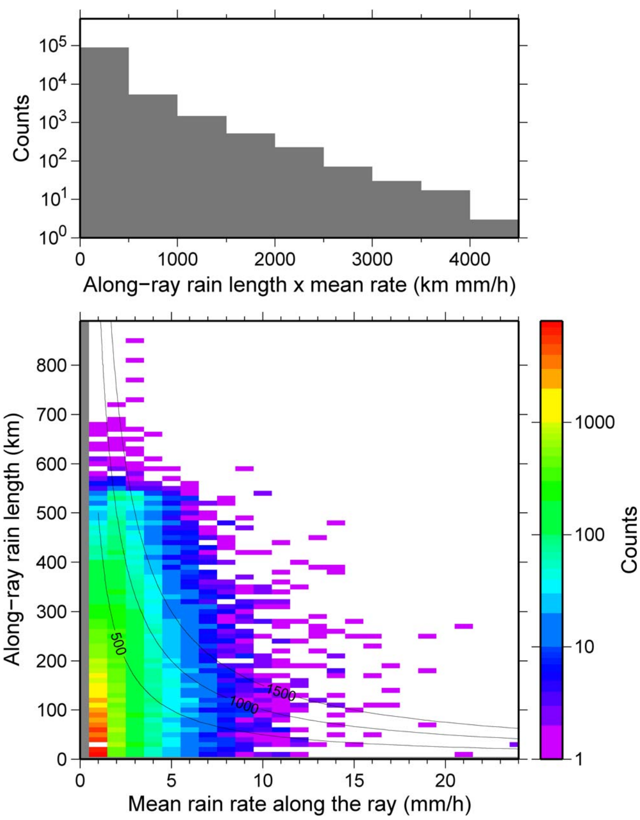

Fig. 7. (Top) Histogram of the ∼420 000 COSMIC events collocated with TRMM for SNR and σ_ϕ analysis, according to a rain scenario value $\langle R\rangle L$. This value is given as the product between the mean rain rate and the total rain length along the radio link. Rain-free events (∼75% of the total events) have not been included. (Bottom) Two-dimensional histogram of the COSMIC events collocated with TRMM (rain-free events not included), according to both main rain rate and total rain length along the radio link. The black contour lines account for the rain scenario as defined by the values in the top panel, up to 1500 mm/h km. Note that these lines separate the different $\langle R\rangle L$-ranges evaluated in Fig. 6.

The phase measurement at each port of PAZ's RO antenna should account for the following terms:

$$\phi_p = \omega t + \phi^{range} + \phi_p^{atm} + \phi_p^{ins} \tag{2}$$

where ω is the carrier frequency, ϕ^{range} is the signature of the phase related to changes in the range between the transmitter and receiver, ϕ_p^{atm} denotes the signatures of the phase due to atmospheric effects in the p-polarization, and ϕ_p^{ins} denotes the signatures in the p-polarization phase induced by instrumental and platform environment.

Given that ϕ_p at each port is expected to be measured with precisions better than or similar to 1 mm (in 1 s) and given that few effects are expected on the amplitude of the signals, the suggested polarimetric observable is the phase shift between both polarization contributions

$$\Delta\phi = \phi_H - \phi_V = \Delta\phi^{atm} + \Delta\phi^{ins} \tag{3}$$

where the carrier (ωt) and range (ϕ^{range}) contributions cancel out, as well as any other effect which is common to both H and V components (most of the atmospheric delay, part of the instrumental induced delay, some of the multipath signatures, etc.).

Because the noise on each port should, in principle, be independent from each other, the precision of the polarimetric phase shift should be $\sqrt{2}$ times the precision at each port. This assumption has been applied in the bottom rows of Table II, to estimate the precision level (at 75 percentile) of the PAZ polarimetric phase-shift measurement. From here on, we assume that PAZ ROHP would be able to detect polarization phase shifts above 1.5-mm delay at the surface level (much finer at higher altitudes), at 1-Hz rate. This estimation only includes the noise level in the phase-delay observations related to the amplitude SNR, and it does not include the remaining systematic effects that could mask the signals, as discussed hereinafter.

A. *Systematic Effects*

Since the observable is a differential phase measurement between the two polarization ports, the following points are true.

1) Any systematic error that induces the same delay or phase effect into both polarizations/ports would cancel out.
2) Any systematic error that introduces a constant and stable bias between both polarizations/ports might be calibrated with extensive sets of rain-free data.
3) Any systematic error that affects differently both polarizations, varies with the geometry, but is constant in time could also be calibrated statistically with rain-free measurements.
4) Any systematic error that affects differently both polarizations and changes with time is a potential threat to detectability.

Points number 2 and 3 can be jointly calibrated in the form of an effective polarimetric phase pattern of the antennas, to be measured during the commissioning phase of the mission. The starting point should be the antenna phase patterns as measured in the anechoic chamber (see bottom panel in Fig. 5), which currently shows differences between the H and V phase patterns between 1.5- and 4-mm shifts for observations around the limb of the Earth, where the precipitation is expected. This corresponds to local spacecraft elevation angles between 21° and 23° and local azimuth between ±50° from the bore-sight.

The assembly of the antenna in the satellite platform might modify this pattern. Multipath might also modify this pattern, introducing systematic phase delays at different regions of the antenna beam. Although multipath tends to affect similarly both polarizations in terms of delay (it clearly affects differently in terms of power), it potentially could introduce phase shifts if the shape and properties of the reflecting surface induce different phase delays to both components. All these local environmental effects will thus be calibrated during the commissioning phase, generating an effective polarization phase-shift antenna pattern, by means of rain-free observations.

Similarly, the effects of the atmospheric multipath will need to be investigated. In principle, atmospheric multipath should not introduce polarimetric features, but it could introduce noise in the phase observables and potential cycle slips. It also acts as a vertical filter, potentially blurring the vertical resolution of the estimates. However, the use of wave optics retrievals could potentially untangle these effects and finally obtain sub-Fresnel vertical resolution.

Electromagnetic signals propagating across the ionosphere suffer a phase shift, the Faraday rotation. In principle, the rotation angle is the same for both polarizations. The ionosphere thus does not introduce a polarimetric phase shift. However, because of this rotation, the vertical and horizontal local axis at the tangent point will not match with the receiver's H/V antenna axis.

Other remaining uncertainties include the stability of certain elements of the system, such as the polarization of transmitted GNSS signals, or the effects of temperature variations in the instrumental delays (ϕ_p^{ins}). It is well known that the platform is exposed to a large range of temperatures. The TurboRogue GNSS receiver, the precedent of PAZ's IGOR receiver, had a reaction of 20-ps delay for each kelvin of variation in the temperature (L. Young, personal communication). This corresponds to 6-mm phase delay/K, which is a significant amount. Again, if the temperature profiles are the same along both port chains, the induced phase delay cancels out in the polarimetric phase-shift observable. However, temperature gradients could leave a nonnegligible residual signature in the polarimetric phase shift. The final impact of this parameter is still unknown, but it will be carefully analyzed during the commissioning phase, making use of the telemetered temperature monitoring information provided by the platform.

In this section, a GNSS RO polarimetric phase observable has been presented, and we estimated that such observable might be measurable by ROHP-PAZ at 1.5-mm precision at 1 Hz and surface level, improving with altitude. A set of systematic effects has been identified, with many of them expected to cancel out. Some of those which might not cancel out could be mitigated and/or monitored. The next question to be answered is whether precipitation events along RO radio links might induce polarimetric phase shifts greater than these expected precision levels.

IV. Precipitation Effects: Forward Models

A forward model is implemented to check the sensitivity of the GNSS L-band polarimetric phase shift to the presence of rain along the propagation path. The approach followed here is the single scattering approximation, under which the forward scattering amplitude f is computed for a single drop of rain, for each value of the drop size. It is then averaged over a distribution of size and angle orientation for a certain shape model. This is a standard approach followed by many authors, as seen in, e.g., [13]. It was also used in [14] to estimate the effect of the rain in the standard (nonpolarimetric) GNSS propagation delay. We here extend [14, eq. (9)] (valid for a particular H- or V-polarization) to the specific differential phase K_{dp}. The specific differential phase is defined as the difference between the phase received at H- and V-polarizations, induced per unit of signal propagation length across the rain. We also multiply it by $\lambda/2\pi$ (with λ being the GNSS carrier wavelength) to obtain the results in units of length rather than radians. We do so because, in the GNSS community, the phase delay is typically given in units of length, through this conversion. In particular, the following specific differential phase results in units of mm of polarimetric differential phase delay per km across the rain (mm-shift/km-rain):

$$K_{dp} = \frac{\lambda^2}{2\pi} \int \Re\left\{f_H(D) - f_V(D)\right\} N(D) dD \tag{4}$$

where $f_H(D)$ and $f_V(D)$ are the forward scattering amplitudes corresponding to the scattering of H- and V-polarized signals off a single D-sized drop, $\Re$ stands for the real part, $N(D)$ is the drop size distribution (also abbreviated DSD hereafter), given in numbers of drops in cubic meter per drop-size interval in mm, and D is the equivolumetric drop diameter in mm.

Similarly to (4), the attenuation suffered by p-polarized signals due to forward scattering per unit of length across rain droplets can be computed as

$$A_p = 20 \log_{10}(e) \lambda \int \Im\left\{f_p(D)\right\} N(D) dD \tag{5}$$

where A_p is the specific attenuation suffered by the p-polarized signal in units of dB-attenuation/km-rain and $\Im$ takes the imaginary part of the forward scattering amplitude. For the reasons explained in Section III, most of the work presented in this study focuses on the polarimetric phase shift rather than attenuations.

The forward (single-) scattering amplitudes f have been computed analytically using the Rayleigh approximation [15] and also numerically following the T-matrix method [16]. Aside from the spherical shape, the analytical expression of the Rayleigh approximation admits simple hydrostatic models of the drop's shape such as oblate spheroids [15]. The numerical approach, of larger computational complexity, permits scattering simulations beyond the Rayleigh regime and more realistic and asymmetric drop shapes, such as the Beard and Chuang (BC) drop shape model [17]. A drop size relationship (DSR), in addition to the shape, is given for all these drop models. The DSR is defined by the axial ratio (AR) between vertical and horizontal sizes as a function of the equivolumetric diameter D; the Pruppacher–Beard (PB) DSR is often used because of the linearity of $AR(D)$ [18]. The scattering dependence with

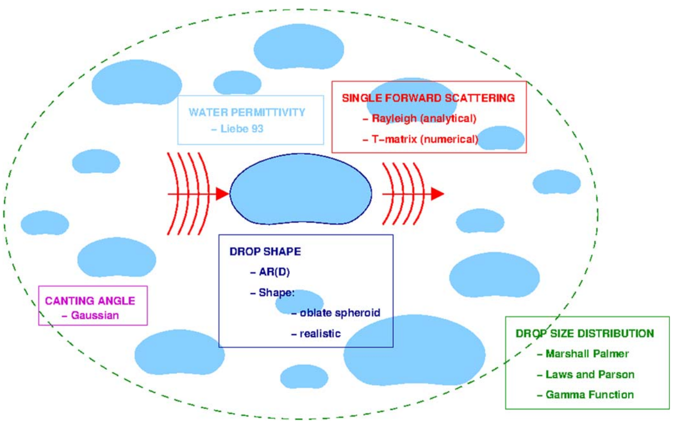

Fig. 8. Sketch of the different models used in the forward model to obtain the specific differential phase K_{dp} and specific attenuation at p-polarization, A_p.

temperature is introduced in the refractive index of the water, using the permittivity model of Liebe *et al.* [19].

Following Oguchi [20], the ensemble average over a Gaussian distribution of the canting angle of the raindrops reduces the differential forward scattering with respect to a vertically oriented medium by a multiplicative factor

$$K_{dp}^{canting} = \frac{1 + e^{-2\sigma_\gamma^2} \cos 2\gamma_0}{2} e^{-2\sigma_\theta^2} K_{dp}^{no-canting} \quad (6)$$

where $K_{dp}^{no-canting}$ is defined in (4), σ_θ^2 is the variance of the canting angle projected on the polarization plane, σ_γ^2 is the variance of the angle between the symmetry axis of the drops and the vertical direction, and γ_0 its mean value. Here, we consider that, in the absence of wind, the drops are effectively canted by the mean angle γ_0 defined between the local vertical plane and the propagation direction (which is only locally horizontal at the tangent point, but it is locally oblique at any other point along the propagation ray path). In all our simulation work, we have set an isotropic deviation of $\sigma_\theta = \sigma_\gamma = 10^\circ$ as the worst case scenario.

Finally, the averaging integral in (4) is based on the DSD $N(D)$, for which different models are available. This study uses the Marshall–Palmer (MP) [21] and the Gamma function model [22]. Fig. 8 sketches the different levels of models involved and their realizations, whereas Table III gives further details. The Python-developed propagation model used here uses core routines of the T-matrix method (implemented in Fortran by Mishchenko [23]) for the numerical calculus of nonspherical-particle scattering.

The resulting specific differential phase K_{dp} for some of these model combinations is shown in Fig. 9, given in mm of polarimetric phase shift per kilometer of propagation through the rain.

K_{dp} is essentially driven by the rain rate R (mm of accumulated water per hour of rain; equivalent to liter per squared meter, per hour of rain). This is directly or indirectly given in the DSD model $N(D)$. The MP model is parametrized by R to describe widespread rain, suitable for area or time averages, whereas the Gamma function model, widely used to describe the DSD variability and for short-term precipitation, has three

TABLE III
MODELS IMPLEMENTED IN THIS STUDY TO ESTIMATE K_{dp} AND THE SIMULATION WORK IN SECTIONS V AND VI

	Drop shape:	
DSR:	Beard-Chuang (BC): $AR(D) = \sum_i a_i D^i$	[17]
	Pruppacher-Beard (PB): $AR(D) = 1.03 - 0.062 \cdot D$	[18]
Shape:	oblate spheroid, used with PB DSR	
	hydrodynamic BC	[17]
	Forward scattering:	
Rayleigh:	analytical	[15]
T-matrix:	T-matrix	[23]
	Drop size distribution (DSD):	
Marshall Palmer (MP):	$N(D) = 8E4e^{-41R^{-0.21}D}[m^{-3}\ cm^{-1}]$	[21]
Gamma Function:	$N(D) = N_0 D^\mu e^{-\Lambda D}$	[22]
	$\Lambda = \frac{3.67+\mu}{D_0}$	
	rain rate from Eq. 7	

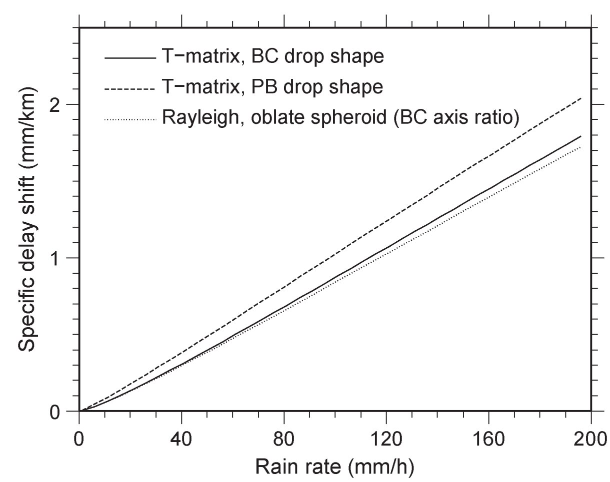

Fig. 9. Specific differential phase K_{dp} for GPS L1 frequency carrier, computed using the MP DSD $N(D)$ at 20 °C of temperature. Both numerical T-matrix and analytic Rayleigh approximation solutions are provided, using three different drop shape models: BC, PB, and oblate spheroid (with axis ratio as given by Beard and Chuang (BC) drop shape model [17]).

input parameters, none of them R. R can be obtained using its definition

$$R = 0.6\pi 10^{-3} \int V_t N(D) D^3 dD \quad (7)$$

where V_t is the terminal speed of the drop (several empirical expressions found, e.g., $V_t(D) = 3.778D^{0.67}$, with D in mm and V_t in m/s [24]).

As explained in Section III, the selected polarimetric GNSS observable is the total difference between the phase delay measured at the H- and the V-ports of the antenna. The rain contribution to this polarimetric phase shift is thus

$$\Delta\phi^{atm} = \int_L K_{dp}(l) dl \quad (8)$$

given in mm when K_{dp} follows (4), where L is the path length of the radio link, $K_{dp}(l)$ is the specific differential phase (in mm/km) at the path length position l [(4) for rain conditions at l, i.e., $R(l)$], and dl is the differential of the path length. K_{dp} is zero in those regions of the radio link where no precipitation is present. For simplicity, we will use the notation $\Delta\phi$ for its rain component $\Delta\phi^{atm}$, hereafter keeping in mind that the actual measured polarimetric phase shift also includes noise and the systematic effects as considered earlier. Because rain occurs at the bottom layers of the atmosphere, these events are always captured around the tangent point in RO observations. Assuming that rain does not happen above 20 km, this sets a limit to the maximum deviation of the local horizontal from the propagation along the ray's precipitation zone to 3°, which is the angle between the local horizontal and the propagation direction at 20-km altitude, along a ray path with its tangent point at the surface level (no bending of the ray trajectory has been considered, which would reduce this angle). Propagation below 20 km will usually be much closer to the local horizontal.

Little literature for L-band forward scattering has been found to compare with the outcome of our implemented models. [14, Fig. 1] presents the specific phase delay for one of the linear polarizations at L1 and L2 GPS frequencies. Our implementation of the model agrees qualitatively with this reference.

A. Retrieval Issues Deduced From the Forward Model

Note that a GNSS link through an intense but localized (small size) rain event might suffer the same polarimetric phase shift as a link through a longer path across lower intensity precipitation. That is, this sole observable cannot, in principle, distinguish between rain rate and length across the rain. We might be tempted to believe that the product of both rate and length across the rain unequivocally determines the polarimetric phase shift. For this to happen, the ratio $K_{dp}(R)/R$ should be constant, which is not the case (as it can be deduced from Fig. 9). Therefore, the ambiguity exists between rain rate, path length across the rain, and even its product. This paper is not intended to solve this question, but possible solutions are suggested. Further studies are required to analyze the following options.

1) If the total attenuation TA of one of the polarizations p could be measured

$$TA_p = \int_L A_p(l)dl \tag{9}$$

then, the ratio $\Delta\phi/TA_p$ would depend only on the rain rate conditions while being independent of the size of the precipitation cell. See the theoretical results of K_{dp}/A_H as a function of the rain rate in Fig. 10 (left). This technique would be suited to separate rain events if TA_p can be properly measured. Because this paper does not tackle the measurability of the rain-induced attenuation TA_p, this is left for future studies.

2) Similarly to the technique behind dual frequency rain gauges [25], the ratio between the polarimetric phase shift measured at both L1 and L2 GPS frequencies might present some sensitivity to the rain rate. Fig. 10 (right) shows K_{dp}^{L1}/K_{dp}^{L2}, which unfortunately is not sensitive to the rain rate (unless differential phase measurements have precisions better than $1^0/_{00}$, which is not the case).

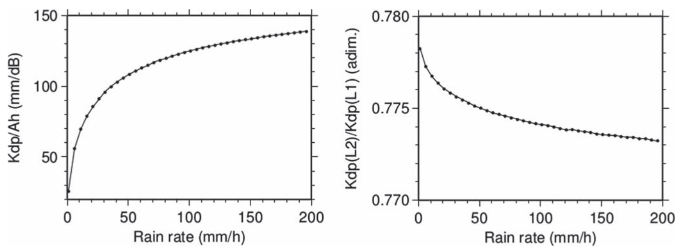

Fig. 10. (Left) Ratio between K_{dp} and A_H (L1 GPS frequency) for different rain rates. (Right) Ratio between K_{dp}^{L1} and K_{dp}^{L2} (with L1 and L2 being the different GPS carrier frequencies).

3) An alternative way to separate the rain rate from the path length across the rain would be through an assimilation scheme into meteorological models.

V. Simulation Case: RO Collocation With TRMM Gridded Products

The former section presented a forward model to estimate the polarimetric differential shift of L-band observations in near-tangential geometry, given an along-ray profile of precipitation, $R(l)$, implicit in (8). Which are the typical or expected rain conditions along the RO rays propagating at the bottom layers of the atmosphere? Are these conditions strong enough to generate differential phases at detectable levels?

In order to answer these questions, a collocation exercise has been conducted between COSMIC RO events and TRMM precipitation gridded products. The TRMM gridded products provide the rain rate on a 2-D grid of $0.25° \times 0.25°$ cells, in 3-h batches (TRMM 3B42 products [26]). The limitations of this data set are summarized as follows.

1) TRMM 3B42 products cover $\pm 60°$ latitude, with no data at high latitudes.
2) No vertical structure is provided by TRMM 2-D products.
3) The resolution of the TRMM grid cells and time batch acts as a filter, lowering the values of the extreme events, thus presenting a smoothed precipitation scenario and losing information on very intense and small or quick events. This might result in *false negative* or *reduced positive* collocations.

We assume that the last two points compensate each other in the global statistics.

In addition to gridded products, TRMM also offers orbital products. These are time tagged according to its measurement time, and some of them include information on the vertical structure of the rain. These characteristics overcome the last three limitations listed earlier. However, it becomes more difficult to find simultaneous and collocated TRMM-COSMIC observations. For these reasons, gridded products have been used to infer a rough estimate of the typical and expected rain conditions of the GNSS RO measurements and, thus, their polarimetric phase observables. Orbital products with vertical precipitation structure information have been included in a separate simulation exercise, detailed in Section VI.

The methodology applied for the simulation study based on 2-D TRMM images is sketched in Fig. 11. For each COSMIC

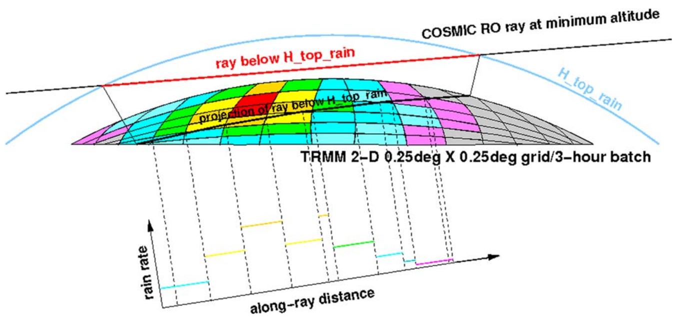

Fig. 11. Sketch of the approach used to collocate COSMIC RO observations against TRMM 2-D gridded products. The goal of this exercise is to determine the along-ray rain profile $R(l)$ corresponding to the rays of the COSMIC RO events at certain fixed altitudes. The vertical extension of the 2-D gridded TRMM precipitation values is assumed to be constant, up to $H_{toprain}$. No bending of the GNSS RO rays has been considered (conservative side).

RO between June 1, 2006 and December 31, 2007, the following steps are performed.

1) A 3-h batch TRMM 3B42 precipitation image is assigned. No time interpolation is performed.
2) For each RO event and presented result, only one of its rays is inspected. It can be the one corresponding to the lowest tangent point or the one corresponding to a given altitude of the tangent point. Note that each RO observation corresponds to a set of different rays at different altitudes, providing vertical scanning capabilities. These capabilities are assessed in the next section.
3) The segment of the straight line below an altitude $H_{top\ rain}$, such that it is oriented as the COSMIC RO radio link and its lowest point corresponds to the RO ray's tangent point, is computed. No bending is considered.
4) The projection of this segment onto the 2-D grid of TRMM rain measurements is performed. The length across each TRMM cell, l_i, and its rain rate R_i are stored to generate COSMIC RO along-ray rain profile $R(l)$.
5) For each crossing cell, the effective mean canting angle α_i is defined as the difference between the local propagation direction and the local horizontal direction. Note that both directions are only coincident at the tangent point of the ray, meaning that it is a function of the along-ray length $\alpha(l)$. This assumes that rain drops fall with their long axis parallel to the local horizontal, and the source of the *effective* canting angle is the nonhorizontal direction of the propagation, rather than drops tilted by wind aerodynamic drag. Therefore, γ_0 in (6) is here equivalent to α. No bending of the ray has been considered.
6) Then, $[R(l), \alpha(l)]$ is used to compute the specific differential phase along the ray path, $K_{dp}(l)$, to finally evaluate $\Delta\phi$ as in (8). The same is done for $A_h(l)$ in (9) to obtain the total attenuation TA_h. In both cases, the T-matrix approach is used, with Beard and Chuang (BC) drop shape [17] and MP DSD.
7) In order to easily classify the events, averages on the along-ray rain rate and rain length are computed. Only precipitating cells are accounted: The along-ray average is defined as $\langle R\rangle = \sum_{R_i>0}(R_i \cdot l_i)/L$ with total crossed rain length $L = \sum_{R_i>0} l_i$. The product $\langle R\rangle L$ is also a suitable indicator for events' classification, as used in Figs. 6 and 7 of Section III.

TABLE IV
NUMBER OF RO EVENTS IN THE COSMIC/TRMM 2-D COLLOCATION EXERCISE THAT REACH DIFFERENT ALTITUDES. ABOVE 3 km, ONLY TROPICAL AREAS ARE CONSIDERED

LATITUDE $\pm60°$ (122,368 RO rain-events)	
Surface level:	77,705
Tangent point at 1 km:	94,794
Tangent point at 2 km:	96,407
LATITUDE $\pm21°$ (43,734 RO rain-events)	
Tangent point at 4 km:	34,446

Approximately a bit more than a quarter of the events show the presence of rain. This represents ~120 000 events between $\pm60°$ latitude.

Two aspects of this methodology require further discussion: the choice of the top-of-the-rain altitude $H_{top\ rain}$ and the noninclusion of ray-bending effects. The typical values of RO bending angles at the bottom layers of the atmosphere are of the order of a few tens of milliradians. On the other hand, the simulation of the bending and applying it into this collocation exercise require further numerical complexity. Moreover, any bending effect would contribute to strengthening the polarimetric signal (longer segments of the ray below a certain altitude and propagation direction closer to the local horizontal), i.e., straight propagation lies on the conservative side of the assessment analysis. For these reasons, it has been considered a second-order effect to analyze in the future on single profiles rather than in this massive statistical study.

As explained earlier, TRMM 2-D gridded data are selected for this exercise, which do not include information about the vertical structure of the precipitation. In midhigh latitudes, rain tends to concentrate in the bottom layers of the troposphere, below ~3 km. At tropical areas, convective rain can reach much higher altitudes, up to 20 km in extreme events.

The vertical extension of the rain has been assumed to be of 6 and 3 km in latitudinal belts: Tropical rain events are assumed to rise up to 6-km altitude, whereas midlatitude events are constrained to the bottom 3 km. The simulations have been conducted at a set of fixed RO ray altitudes: surface altitude ($h = 0$), $h = 1$ km above the surface, $h = 2$ km, and $h = 4$ km altitude (this latter in the tropics solely).

A. *Two-Dimensional Collocation Simulation Results*

Some of the ~120 000 RO rain events do not reach the bottom layers of the troposphere. This is a consistent feature of all RO missions: As the occultation gets down to the atmosphere, superrefractive layers, local topography, and multipath might arise and hinder the receiver to track the GNSS signal. As a consequence, it is well established that a percentage of RO is lost in the lowermost atmospheric depths. Table IV summarizes the COSMIC ROs within our collocation exercise that reach different altitudes.

The main result of this collocation exercise is shown in Fig. 12. On the top panel, the ~78 000 collocated events that

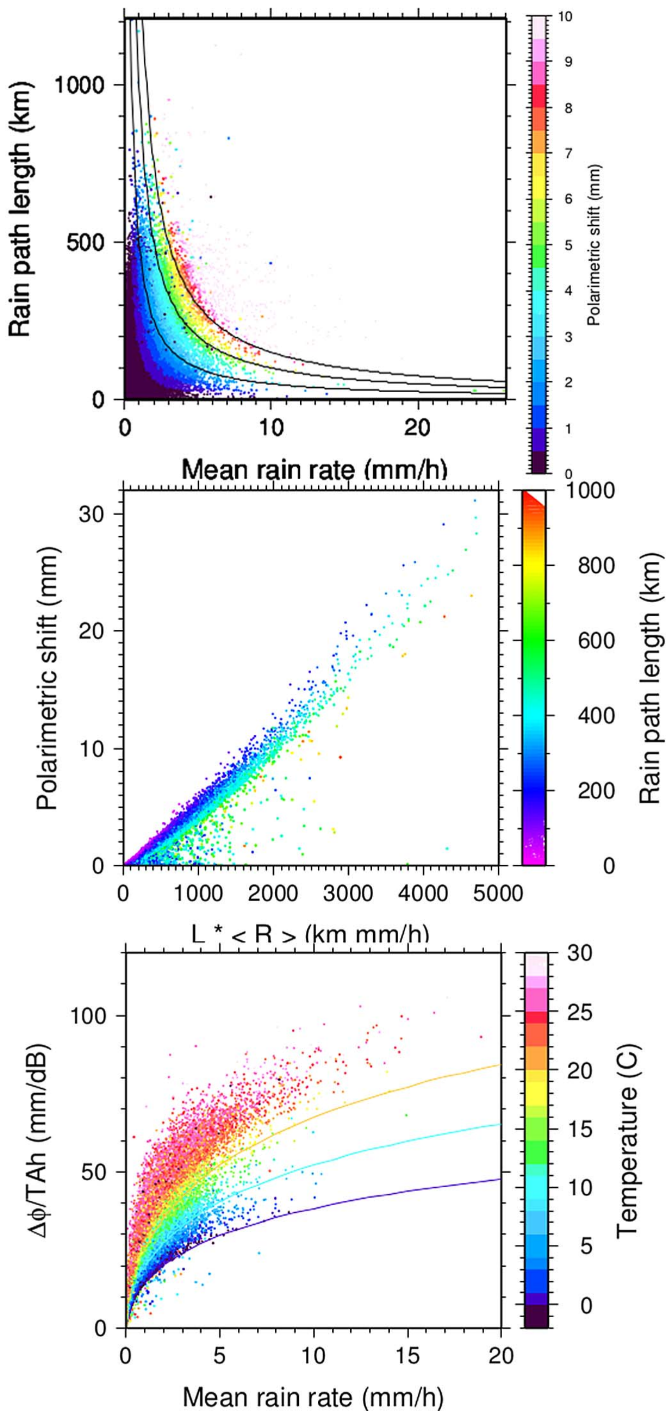

Fig. 12. Results of the simulation using 2-D collocated events, for rays with tangent point at surface level. (Top) Polarimetric phase shift induced by the rain conditions occurring along the collocated rays $R(l)$. They are plotted according to their mean rain rate $\langle R\rangle$ and total rain length L along the rays. Solid black lines indicate constant values of the product $\langle R\rangle L$. (Middle) Polarimetric phase shift as a function of the product $\langle R\rangle L$. (Bottom) Ratio between the observables $\Delta\phi$ and TA_h, as a function of the mean rain rate along the ray path $\langle R\rangle$. Color scale for temperature. Solid lines for the ratio between the specific variables K_{dp}/A_h.

reach the surface level are displayed as a function of their average rain $\langle R\rangle$ and total rain length L along the ray path. The color scale shows the polarimetric phase induced along each of these rays. As summarized in Table II, the expected precision of the polarimetric shift observable at surface level is in the range of 1–1.4 mm. Therefore, any events in the upper panel of Fig. 12 plotted in the two or three darker shades of blue would not be detectable. The rest of the events would present polarimetric-shift signatures above the noise level, thus detectable. Those correspond to both intense and light rates of rain, of different horizontal extent sizes. The magnitude of the polarimetric signature seems to relate with the product $\langle R\rangle L$. However, as shown in the central panel of the figure, the correlation between $\langle R\rangle L$ and the polarimetric shift is strong, but not perfect: For a given $\langle R\rangle L$ value, intense and localized events tend to present a higher polarimetric shift than weaker but broader precipitation scenarios. Finally, the bottom panel of the figure presents the results of the simulated $\Delta\phi/TA_h$, which could help in separating the rain rate from the rain extension information. This ratio is a function of the temperature (color scale in the bottom panel). It is worth highlighting that the ratio $\Delta\phi/TA_h$, as a function of $\langle R\rangle$, follows the ratio of their specific counterparts K_{dp}/A_h (solid lines in the bottom panel). The atmospheric temperature profile is known in RO observations, being one of the standard products of the technique, although under moist/rain conditions, temperature uncertainties are larger than that under dry conditions. A separate study—left as future work—should address the feasibility of measuring attenuation and whether the precision of the temperature profiles given by standard-RO profiles (or other temperature products, e.g., NWPM global reanalysis) under rainy conditions is sufficient to untangle rain and rain extension using this technique.

Part of the dispersion in the top panel of Fig. 12 might be due to the variability of rates within the rain profile along the ray $R(l)$ while being plotted as a function of the average rain rate along the ray $\langle R\rangle$. Fig. 13 shows the differences between this plotting approach (left panel) and plotting the same data set as a function of the maximum rain rate within the ray $Max(R(l))$ (central panel). This latter plot presents further dispersion: The maximum rain rate within the ray path is less representative of the total polarimetric phase shift than the average rain rate along the ray path. It also shows that these simulation exercises included rain cells of up to 50-mm/h precipitation rate. To complete this comparison, the right panel presents similar plots, but computed with the average rain rate and rain length rather than the integral of the actual rain profile along the ray path [see (8)]. The comparison between the left and right panels in Fig. 13 thus shows that the dispersion in the left (and top of Fig. 12) is generated by the diversity of rates within the rain profile along the ray path.

We could only find a weak (poorly significant) seasonal pattern in the polarimetric RO observations at midlatitudes (between 30° and 60°). This pattern is slightly more clear in the northern hemisphere, where the polarimetric observable acquires stronger values by the end of summer and during the fall.

Unlike the seasonal pattern, the geographic patterns are strong. As shown in Fig. 14, strong polarimetric observables are induced by rain events along areas with heavy precipitation events: around the Equator and over other masses of hot sea surface water. In some broad zones such as South-East of the Oceans (SEO), characterized by colder waters, the rain-induced

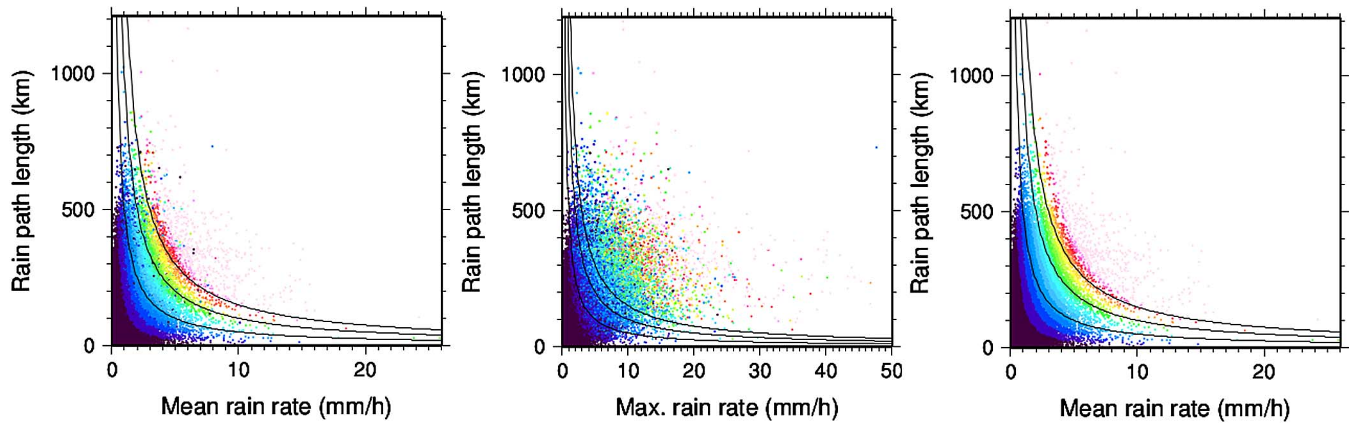

Fig. 13. Color scale in Fig. 12 (top). (Left) Same as Fig. 12, for rays with their tangent point at 1-km altitude. (Center) Same data as in the left panel, but plotted as a function of the maximum rain rate along the ray path: $Max(R(l))$. (Right) Same as left panel, but simulations computed directly with the mean quantities, not with the along-ray profiles $R(l)$. That is, $\Delta\phi = K_{dp}(\langle R\rangle)L$ rather than the integral along the ray [see (8)].

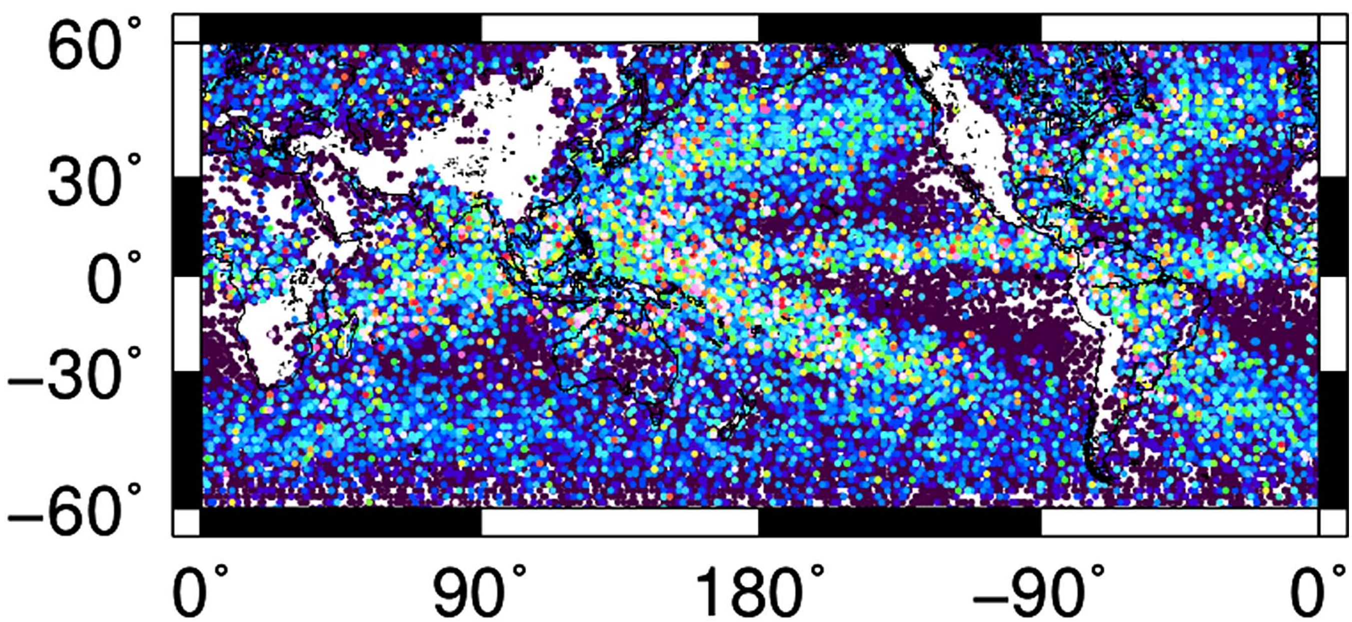

Fig. 14. Map of the ∼78 000 COSMIC rain events at surface level, with the presence of rain. The color code corresponds to the polarimetric observable $\Delta\phi$, following the color scale in Fig. 12 (top). Most of the strong polarimetric phase shift concentrates in areas of intense precipitation. Some areas over colder water masses (e.g., SEO) present rain events below the detectability threshold only (dark blue).

polarimetric shift is $\Delta\phi \leq 0.5$ mm (darker blue), below the detectability level.

Ultimately, this simulation exercise based on COSMIC/TRIMM 2-D collocations permits to obtain a rough estimate of the type of events to which PAZ polarimetric observations will be sensitive, together with the frequency of their occurrence: Approximately 90% of the events with the average rain rate higher than 5 mm/h have shown polarimetric signatures above the noise level of the observation and are therefore detectable (see Table V). In general, both moderate to intense precipitation events, in a wide range of horizontal extensions, induce detectable levels of polarimetric phase shift, but heavier rain tends to induce stronger polarimetric observables, as identified in the geographical map.

TABLE V
PERCENTAGE OF RAIN-RO EVENTS IN THE COSMIC/TRMM 2-D COLLOCATION EXERCISE THAT RESULT IN A POLARIMETRIC PHASE SHIFT ABOVE THE DETECTABILITY LEVEL (1.5-mm SHIFT, CONSERVATIVE THRESHOLD IN TABLE II). PERCENTAGES OF DETECTABILITY ARE GIVEN FOR DIFFERENT RAIN INTENSITIES (ALONG-RAY AVERAGED)

Precipitation intensity $< \mathbf{R} >$:	**Percentage of detectable cases**
$>$ 0.5 mm/h	24 %
$>$ 1 mm/h	41 %
$>$ 2 mm/h	72 %
$>$ 3 mm/h	83 %
$>$ 4 mm/h	88 %
$>$ 5 mm/h	90 %
$>$ 10 mm/h	95 %

The collocation of COSMIC RO with TRMM 2-D rain products has resulted in a statistical indication of the sort of events that would be detectable with PAZ polarimetric RO instrument. To do so, only a few rays of the RO have been inspected, typically the closest to the surface, and the vertical structure of the precipitation has not been considered.

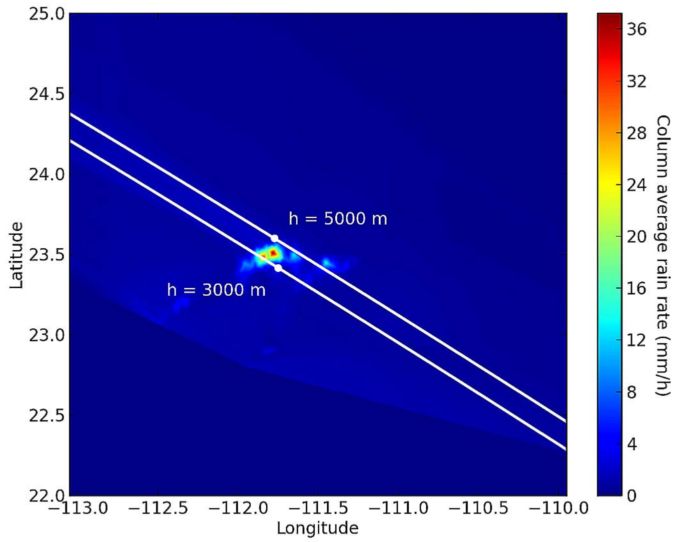

Fig. 15. TRMM event selected for a 3-D simulation (September 23, 2007), plotted here as a 2-D image of the average rain rate along the vertical column. Two rays of a geocollocated COSMIC RO event are overlaid, corresponding to different altitudes of the tangent point (white dots). Below 5-km altitude, there are almost 600 of such rays—not plotted here. Note that the simulation of the effect of the precipitation is made using the 3-D TRMM rain rate information, not its vertical average.

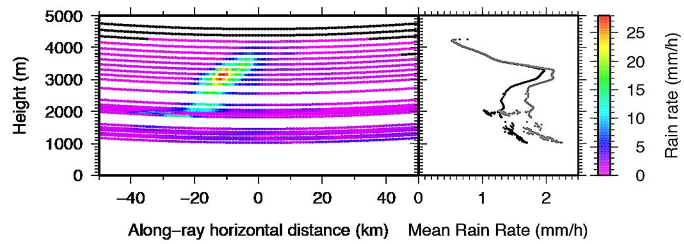

Fig. 16. (Left) Along-ray rain profiles as extracted from geographical collocation of the TRMM 3-D precipitation event with COSMIC RO in Fig. 15. They are plotted as a function of altitude to highlight that different points of the same ray lie at different altitudes, but close to horizontal-looking geometry. Every COSMIC RO event (as it will be for PAZ RO) is formed by thousands of such rays, at 20-ms sampling interval. For clarity purposes, only a few of them have been plotted here (1 out of 20 rays; this is 1 every 400 ms). Rain rate color scale on the right; black for rain-free segments. (Right) Along-ray average rain rate (zero rain not accounted in the average), computed using (black) 1000-km ray length and (gray) 200-km ray length for all COSMIC RO available rays below 5-km altitude.

VI. Simulation Case Using TRMM 3-D Precipitation Structures

The RO technique performs a time series of measurements as the radio link or ray descends vertically through the atmosphere. In both COSMIC and PAZ RO missions, the sampling rate is 50 Hz, i.e., one measurement every 20 ms. For the purposes here, we can assume that each of these measurements comes from a radio link or ray. To obtain the desired level of precision, a running-window averaging of 1-s width should be applied. This time resolution corresponds to a vertical resolution in the range between 150 and 500 m in the bottom 5 km of the troposphere, which is finer at lower altitudes. This vertical resolution is of the order or larger than the vertical extent of the Fresnel volume, of the order of 100 m. In order to understand and illustrate the potential use of the time series of polarimetric observables within a single RO event and as a tool for the vertical scanning of the rain, one collocation between COSMIC RO and TRMM 3-D rain products (orbital products, TRMM 2B31 [26]) has been analyzed, simulating the polarized RO signals at 50-Hz sampling rate, after a 1-s running-window averaging. We have looked for geographical collocation solely (not in time) because the purpose of this exercise is not statistical but an illustrative simulation of how the time series of RO polarimetric measurement would look.

We have looked for a COSMIC RO with tangent points of the lowest rays within the main rain area of the selected TRMM 3-D precipitation event and the RO plane (orientation of the radio link) nearly parallel to the TRMM orbital ground track. The selection of the event was rather random, beyond looking for a relatively intense rain confined in a relatively small region. The selected case took place on September 23, 2007 at $\sim$23.5° N, -112° E, over the Pacific Ocean: The rain rate given by TRMM takes values of up to 28 mm/h over extensions of several kilometers. Fig. 15 displays the location of the selected TRMM event and two of the COSMIC RO rays scanning the area. Then, a ray tracer is used to estimate the trajectory of each ray of the COSMIC RO 20-ms observation. Note that the ray location moves in time as the tangent point drops its altitude. As a consequence, the scanning of the precipitation cell does not correspond to a vertical slice but to a slant slice. The ray tracer is Occultation Analysis Tools (OAT) [27] and solves the ray trajectory across an atmosphere characterized by the refractivity profile corresponding to the COSMIC event under analysis. This is not the exact refractivity profile corresponding to the rain event because there is no time collocation, but the differences in the bending of the rays are expected to be small and irrelevant for the illustrative purposes of this exercise. Unlike the former collocation exercise, the rays are bent in this simulation. For each j-ray of the time series t^j, we keep the coordinates of 1000 points around the tangent point ($\pm$500 from the tangent point), spaced 1 km along the ray. This set of i-points ($i = 1 \cdots 1000$) define the along-ray path distance l_i as well as the angle between the local horizontal and the propagation direction, angle α_i. Finally, the TRMM 3-D rain product is interpolated at the set of l_i points. In this way, the along-ray rain rate series $R(l_i)$ and propagation misalignment $\alpha(l_i)$ are produced.

The simulation generates as many along-ray rain rate series $(R^j(l_i); \alpha(l_i))$ as RO measurements at 20-ms rate in a single event: $j = 1 \cdots M$. Their altitude gradually decreases with time t^j. Each of these rays have one single lowest altitude point (tangent point of altitude h^j_{tan}), but the rest of the ray points are at higher altitudes. Below 5-km altitude, the selected COSMIC RO event is the compound of M $\sim$580 20-ms measurements/rays gradually lowering their tangent point. This vertical scan takes less than 15 s. Fig. 16 shows the interpolated rain rate along different rays in a single RO event, plotted as a function of the altitude of each ray point. For clarity purposes, only some of these j-rays have been plotted.

The forward model described in Section IV is then applied to each ray of the RO event, also using information about the vertical profile of atmospheric temperature given by the standard COSMIC RO products. In this way, the polarimetric phase shift induced by the rain along each ray is estimated:

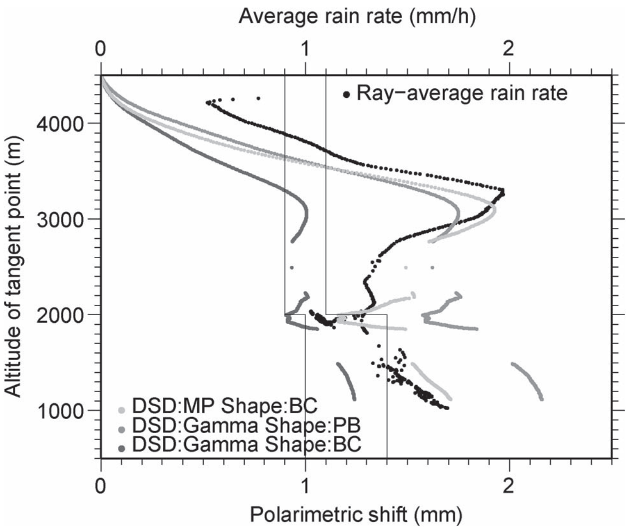

Fig. 17. Polarimetric phase shift $\Delta\phi$ induced by rain on each j-ray (20-ms sampling) after 1-s filter is applied, corresponding to the COSMIC RO event geographically collocated with the TRMM 3-D precipitation product in Fig. 15. It has been plotted as a function of the altitude of the tangent point for each j-ray, h^j_{tan}. $\Delta\phi^j$ has been computed applying the integral equation (8) according to three different models (different hues of gray; units given in bottom x-axis) to each ray independently and later 1 s averaged. For comparison, the black profile is the along-ray averaged rain rate (units given in top x-axis). The two detectability thresholds obtained in the bottom half of Table II are marked with thin solid vertical lines. The expected detectability is expected to be in between the two of them.

$\Delta\phi^j$. A 1-s filter is then applied to take into account the time-averaging window required to improve the precision of the polarimetric phase observations. Fig. 17 shows the resulting observables, as a function of the tangent point altitude of each j-ray. Three different models have been used: combinations of either Gamma function (D_0 set to 1 mm and μ set to 3) or MP DSD, with DSR by BC or PB. Most of the event would be detectable from RO data according to two of the models (Gamma DSD with PB DSR and MP distribution with BC shape ratio), whereas it would be below detectability according to this particular Gamma DSD with BC DSR. This indicates that it will be crucial to identify the most realistic models for this technique under different precipitation scenarios.

The exercise also shows good qualitative agreement between the vertical profile of the along-ray averaged rain rate and the measured polarimetric shift: The polarimetric-shift profile obtained with the three models captures the structure of the along-ray path-averaged rain rate.

VII. Summary and Conclusion

This paper has first presented the polarimetric RO mission to be conducted aboard the PAZ LEO: the ROHP-PAZ experiment, planned to be launched in 2014. This will be the first spaceborne polarimetric RO payload, intended to prove the capabilities of a new measurement concept based on polarimetric RO. The focus of this work is to find the sensitivity of these signals of opportunity for remote sensing of intense atmospheric precipitation events. An IGOR+GNSS RO receiver is the main RO payload, together with an antenna with to linear polarization ports (H/V). The second part of this paper presents a theoretical feasibility study: It simulates the response of the observables and their expected noise levels. We presented the forward models to estimate rain-induced effects on the observables, and finally, a set of COSMIC RO events collocated with TRMM rain products have been used as a base for simulation work to assess their detectability.

The observable explored here is the difference between the phase delay measured at each port of the polarimetric antenna (H and V ports). We have called it polarimetric phase shift $\Delta\phi$. One of the reasons for this selection is that GNSS receivers track the phase of the signals very precisely and can measure very precisely the variations in the ranges. The estimation of the expected noise level in the polarimetric RO observables has been based on the analysis of phase noise levels in actual COSMIC RO data, which has been conservatively extrapolated to the PAZ scenario. At near Earth-surface level, the expected polarimetric phase-shift noise is at 1.5-mm level or better after 1-s averaging, improving with altitude. The systematic effects have been listed but not quantified. We argue why most of them may be calibrated during the commissioning phase, as part of characterizing the antenna transfer function or its effective polarimetric phase pattern.

The forward model to assess the impact of rain onto the polarimetric phase shift is based on the forward scattering amplitude under the single scattering approximation. The approach is rather standard, and we have implemented an existing T-matrix numerical computation code as core routines for our simulations. Among a diversity of available models, we have selected a few of them, which are widely used by the community (MP and Gamma function DSDs, BC and PB drop shapes and shape ratios, and Rayleigh analytical on oblate spheroid drop shapes).

Two simulation experiments have been presented: the first one was based on more than 400 000 COSMIC RO events collocated with TRMM 3-hourly batched and 2-D gridded rain information, of which 120 000 events presented rain along the RO ray path. The second experiment corresponds to a single COSMIC RO profile collocated with TRMM 3-D rain structures. The goal of the first exercise is statistical—to answer questions about what type of rain events would result in observables above the detectability threshold and in what percentage. The results have shown that the polarimetric phase-shift observable cannot distinguish between intense rain in reduced extension and light rain in extended areas. High values of the polarimetric observable are typically associated with more intense rain, as captured in the geographical distribution of $\Delta\phi$, showing most of the strong polarimetric shifts concentrated in areas of intense precipitation. The study also shows that heavy precipitation events are more easily detected than light rain. For instance, among all the events with along-ray averaged rain rates higher than 5 mm/h, 90% of them resulted in detectable $\Delta\phi$ levels.

The second exercise, using TRMM 3-D rain products, is meant to illustrate the vertical profiling capabilities of the technique. The $\Delta\phi$ observable has been simulated for each 20-ms RO measurement/ray and then averaged to 1 s. Because each of these measurements crosses the atmosphere tangentially at different altitudes, it results in a series of $\Delta\phi$ as a function of altitude. This vertical profile of the polarimetric phase shift has been shown to capture the structure of the along-ray averaged rain rate given by the TRMM collocation.

The study demonstrated the detectability of intense atmospheric precipitation events. The sole achievement of flagging profiles of atmospheric temperature within optically thick clouds with information about the precipitation state is relevant to atmospheric scientists, complementing the future PAZ RO atmospheric thermodynamic profiles with a rain flag. Additional modeling being done at the current time includes the modeling of the effect of ice crystals using the discrete dipole approximation [28] and improved assumptions to model mixed phase and melting regions typical of convective and stratiform precipitation, respectively, neither of which were considered in this initial study. If unique differential phase signatures are noted in and near the freezing level, this information could potentially be useful to NWP models which will assimilate ROHP data since these models carry different parameterizations to convert condensation between liquid and ice phases for convective and stratiform rainfall conditions.

One of the essential limitations is the horizontally integrated nature of the RO observations. It is shown that the use of signal attenuation parameters can help separate the rain rate from the rain cell size, but this study did not investigate the feasibility of properly measuring the rain-induced attenuation from polarimetric GNSS RO. This is also left as future work. Alternative approaches to disentangle the horizontally integrated information might rely on external data, tomographic approaches, or model-assimilation schemes. Along this line of research, appropriate forward model operators should be implemented, and impact studies should be performed.

The combination of RO horizontal glimpses of rain with other types of nadir-looking rain measurements has the potential to complement each other. The PAZ mission will overlap with the expected launch of the GPM mission, with its core satellite dual-frequency (Ku-/Ka-band) precipitation radar (DPR). The DPR is expected to provide improved separation of the vertical particle phase, liquid water content, and DSD parameters, which will allow for more realistic modeling of time/space-coincident ROHP observations, relative to assumptions made with the single-frequency TRMM radar. This synergy may make PAZ a unique complimentary mission by enabling the simultaneous observation of the thermodynamic temperature and moisture profile directly within precipitating clouds, a capability which is not possible from current passive microwave or infrared sounders such as the Atmospheric Temperature and Moisture Sounder and the AIRS, respectively. The PAZ orbit is near polar, which ensures dense coverage over the 65° orbit inclination of the GPM core satellite.

ACKNOWLEDGMENT

The authors would like to thank HISDESAT and the Radio-Occultation and Heavy Precipitation with PAZ International Scientific Team for their support. The authors would also like to thank L. E. Young (NASA/Jet Propulsion Laboratory (JPL)) and the Broadreach Engineering staff for their valuable comments and information.

REFERENCES

[1] S. B. Healy, A. M. Jupp, and C. Marquardt, "Forecast impact experiment with GPS radio occultation measurements," *Geophys. Res. Lett.*, vol. 32, no. 3, pp. L03804-1–L03804-4, Feb. 2005.

[2] L. Cucurull and J. C. Derber, "Operational implementation of COSMIC observations into NCEP's global data assimilation system," *Weather Forecast.*, vol. 23, no. 4, pp. 702–711, Aug. 2008.

[3] C. Cardinali, *Forecast Sensitivity to Observation (FSO) as a Diagnostic Tool*. Reading, U.K.: European Centre for Medium-Range Weather Forecasts, 2009, ser. ECMWF Tech. Memo. 599.

[4] "A community assessment and strategy for the future, earth science and applications from space, national imperatives for the next decade and beyond," The National Academies Press, Washington, DC, USA, 2007.

[5] R. Peters, P. Woolner, and E. Ekelman, "Analytic calculation of noise power robbing, NRP, polarization isolation degradation," in *Proc. 26th AIAA ICSSC*, San Diego, CA, USA, Jun. 2008. DOI: 10.2514/6.2008-5509.

[6] F. J. Wentz, L. Ricciardulli, K. Hilburn, and C. Mears, "How much more rain will global warming bring?" *Science*, vol. 317, no. 5835, pp. 233–235, Jul. 2007.

[7] R. P. Allan and B. J. Soden, "Atmospheric warming and the amplification of precipitation extremes," *Science*, vol. 321, no. 5895, pp. 1481–1484, Sep. 2008.

[8] Q. Yue *et al.*, "Cloud-state-dependent sampling in AIRS observations based on CloudSat cloud classification," *J. Clim.*, vol. 26, no. 21, pp. 8357–8377, Nov. 2013.

[9] *WMO Manual on Codes*, World Meteorological Organization, Geneva, Switzerland, 2011.

[10] B.-H. Wu, V. Chu, P. Chen, and T. Ting, "FORMOSAT-3/COSMIC science mission update," *GPS Sol.*, vol. 9, no. 2, pp. 111–121, Jul. 2005.

[11] G. Beyerle *et al.*, "First results from the GPS atmosphere sounding experiment TOR aboard the TerraSAR-X satellite," *Atmos. Chem. Phys.*, vol. 11, no. 13, pp. 6687–6699, Jul. 2011.

[12] H. G. Tompkins and E. A. Irene (ed.), *Handbook of Ellipsometry*. Norwich, NY, USA: William Andrew Publishing, 2005, p. 870.

[13] R. L. Olsen, "A review of theories of coherent radio wave propagation through precipitation media of randomly oriented scatterers, the role of multiple scattering," *Radio Sci.*, vol. 17, no. 5, pp. 913–928, Sep./Oct. 1982.

[14] F. S. Solheim, J. Vivekanandan, R. H. Ware, and C. Rocken, "Propagation delays induced in GPS signals by dry air, water vapor, hydrometeors, other particulates," *J. Geophys. Res.*, vol. 104, no. D8, pp. 9663–9670, Apr. 1999.

[15] A. Ishimaru, "Scattering and absorption by a particle," in *Wave Propagation and Scattering in Random Media*, vol. 1. Neq York, NY, USA: Academic, 1978, pp. 18–22.

[16] M. I. Mishchenko, L. D. Travis, and D. W. Mackowski, "T-matrix computations of light scattering by nonspherical particles: A review," *J. Quant. Spectrosc. Radiat. Transf.*, vol. 55, no. 5, pp. 535–575, May 1996.

[17] K. V. Beard and C. Chuang, "A new model for the equilibrium shape of raindrops," *J. Atmos. Sci.*, vol. 44, no. 11, pp. 1509–1524, Jun. 1987.

[18] H. Pruppacher and K. V. Beard, "A wind tunnel investigation of the internal circulation and shape of water drops falling at terminal velocity in air," *Q. J. R. Meteorol. Soc.*, vol. 96, no. 408, pp. 247–256, Apr. 1970.

[19] H. J. Liebe, A. G. Hufford, and M. G. Cotton, "Propagation modeling of moist air and suspended water/ice particles at frequencies below 1000 GHz," presented at the Proc. NATO/AGARD Wave Propagation Panel 52nd Meeting, Palma de Mallorca, Spain, May 17–20, 1993, Paper 3/1-10.

[20] T. Oguchi, "Electromagnetic wave propagation and scattering in rain and other hydrometeors," *Proc. IEEE*, vol. 71, no. 9, pp. 1029–1078, Sep. 1983.

[21] J. S. Marshall and W. M. Palmer, "The distributions of raindrops with size," *J. Meteorol.*, vol. 5, no. 4, pp. 165–166, Aug. 1948.

[22] C. W. Ulbrich, "Natural variations in the analytical form of the raindrop-size distribution," *J. Clim. Appl. Meteorol.*, vol. 22, no. 10, pp. 1764–1775, Oct. 1983.

[23] [Online]. Available: http://www.giss.nasa.gov/staff/mmishchenko/t_matrix.html

[24] D. Atlas and C. W. Ulbrich, "Path- and area-integrated rainfall measurement by attenuation in the 1–3 cm band," *J. Appl. Meteorol.*, vol. 16, no. 12, pp. 1322–1331, Dec. 1977.

[25] R. F. Rincon and R. H. Lang, "Microwave link dual-wavelength measurements of path-average attenuation for the estimation of drop size distributions and rainfall," *IEEE Trans. Geosci. Remote Sens.*, vol. 40, no. 4, pp. 760–770, Apr. 2002.

[26] Precipitation Processing System Tropical Rainfall Measuring Mission, File Specification for TRMM Products, p. 328, Dec. 2012. [Online]. Available: http://pps.gsfc.nasa.gov/Documents/filespec.TRMM.V7.pdf

[27] J. M. Aparicio and A. Rius, "A raytracing inversion procedure for the extraction of the atmospheric refractivity from GNSS travel-time data," *Phys. Chem. Earth*, vol. 29, no. 2/3, pp. 213–224, 2004.

[28] B. T. Draine and P. J. Flatau, "Discrete dipole approximation for scattering calculations," *J. Opt. Soc. Amer. A, Opt. Image Sci.*, vol. 11, no. 4, pp. 1491–1499, Apr. 1994.

Estel Cardellach (M'10) received the Ph.D. degree from the Polytechnic University of Catalonia, Barcelona, Spain, in 2002.

She has been working on scientific applications of the Global Navigation Satellite System (GNSS) for remote sensing of the Earth, such as the extraction of geophysical information of the GNSS reflected signals, radio occultation, and geodetic techniques. She was a National Research Council Awardee for a postdoctoral position at NASA/Jet Propulsion Laboratory, Pasadena, CA, USA, in 2002–2003 and a Postdoctoral Researcher at the Harvard Smithsonian Center for Astrophysics, Cambridge, MA, USA, in 2003–2005. Since 2005, she has been at the Institute of Space Sciences (ICE-Consejo Superior de Investigaciones Científicas/Institut d'Estudis Espacials de Catalunya), currently under the Spanish Ramón y Cajal program. She is the local manager of EUMETSAT's Radio-Occultation Meteorology Satellite Application Facility. She is the PI of the spaceborne experiment *Radio-Occultation and Heavy Precipitation* aboard the PAZ low Earth orbiter and a member of the *GNSS Reflectometry, Radio Occultation and Scatterometry experiment aboard the International Space Station* Proposing Team and Scientific Advisory Group. She has been appointed Cochair of the IEEE GRSS GNSS Working Group, under the Instrumentation Future Technologies Technical Committee.

Sergio Tomás received the M.S. and Ph.D. degrees in telecommunication engineering from the Universitat Politécnica de Catalunya, Barcelona, Spain, in 2005 and 2011, respectively, doing his undergraduate thesis at the Institute of Photonic Sciences (ICFO) in Barcelona.

In 2012, he joined the Institute of Space Sciences (ICE-Consejo Superior de Investigaciones Científicas/Institut d'Estudis Espacials de Catalunya) in Bellaterra, Spain, as a Research Engineer to work on the detection of precipitation with polarimetric GNSS radio occultations (ROs). His research interests include LIDAR remote sensing, related signal processing for wind monitoring and boundary layer detection, atmospheric turbulence, and GNSS ROs for precipitation detection.

Santi Oliveras is an Electronics Engineer in telecommunications from the Universitat Politécnica de Catalunya, Barcelona, Spain, in 2002. He has been at the ICE-Consejo Superior de Investigaciones Científicas/Institut d'Estudis Espacials de Catalunya since 2004, as a member of EUMETSAT's GRAS Satellite Application Facility project, related to GPS radio ocultations. Within ICE-Consejo Superior de Investigaciones Científicas/Institut d'Estudis Espacials de Catalunya's Earth Observation group, he is also involved in other projects related to remote sensing using Global Navigation Satellite System signals.

Ramon Padullés received the B.S. degree in physics and the M.S. degree in astrophysics, cosmology, and particle physics from the University of Barcelona, Barcelona, Spain. Since 2012, he has been working toward the Ph.D. degree on precipitation measurements with polarimetric Global Navigation Satellite System radio occultations in the Institute of Space Sciences (Consejo Superior de Investigaciones Científicas/Institut d'Estudis Espacials de Catalunya).

He is under the *Formación de Personal Investigador* fellowship from the Spanish government and he has also participated in the JPL Visiting Student Researchers Program at the NASA/Jet Propulsion Laboratory, Pasadena, CA, USA. He is currently involved in the analysis of the data from the polarimetric ground campaign experiment and in the simulation of hydrometeor effects on the polarimetric signal within the framework of the Radio-Occultation and Heavy Precipitation with PAZ mission.

Antonio Rius (M'00) received the Ph.D. degree in astrophysics from Barcelona University, Barcelona, Spain, in 1974.

From 1975 to 1985, he was a member of the Technical Staff at NASA's Deep Space Communications Complex, Madrid, Spain, where he was responsible for the radio astronomical activities. Since 1986, he has been with the Spanish Consejo Superior de Investigaciones Científicas (CSIC), Barcelona. He is currently a CSIC Research Professor AH, working within the research group on Earth Observation at the Institut d'Estudis Espacials de Catalunya (ICE-CSIC/Institut d'Estudis Espacials de Catalunya).

Manuel de la Torre-Juárez, photograph and biography not available at the time of publication.

Francis Joseph (Joe) Turk received the B.S and M.S degrees in electrical engineering from Michigan Technological University, Houghton, MI, USA, and the Ph.D. degree in electrical engineering from Colorado State University, Fort Collins, CO, USA.

He has a broad background in science, applications, algorithms of observations from satellite and aircraft-based microwave radar and radiometric instruments, polarimetric weather radar observations, radio wave propagation, and radar and radiative transfer modeling. From 1995 to 2008, he was with the Naval Research Laboratory's Marine Meteorology Division. He is currently a member of the NASA Precipitation Measurement Missions science team and an Editor of the AMS Journal of Hydrometeorology.

Dr. Turk has been a recipient of two NASA Group Achievement Awards and four Alan Berman publication awards.

Chi O. Ao received the A.B. degree in physics from the University of California at Berkeley, CA, USA, in 1993 and the Ph.D. degree in physics from the Massachusetts Institute of Technology, Cambridge, MA, USA, in 2001. He joined the Tracking System and Applications Section at the NASA Jet Propulsion Laboratory, Pasadena, CA, USA, in 2001 and has worked on various aspects of Global Positioning System (GPS) radio occultation (RO) since then. He has extensive experience in GPS RO inversion techniques and simulation methods and has a strong interest in the climate applications of RO data. He is the principle investigator and coinvestigator of several NASA grants and is currently a member of the NASA Global Navigation Satellite System Science Team and the CLARREO Science Definition Team.

E. Robert Kursinski, photograph and biography not available at the time of publication.

Bill Schreiner, photograph and biography not available at the time of publication.

Dave Ector, photograph and biography not available at the time of publication.

Lídia Cucurull received the Ph.D. degree in physics, with specialty in atmospheric sciences, on the use of Global Navigation Satellite System signals in numerical weather prediction from the Barcelona University, Barcelona, Spain, in 2001.

Since then, she has worked at the University Corporation for Atmospheric Research, Boulder, CO, USA, the NASA Goddard Space Flight Center, Greenbelt, MD, USA, the National Oceanographic and Atmospheric Administration (NOAA) National Weather Service, Silver Spring, MD, USA, and the NOAA National Environmental Satellite, Data and Information Services, Suitland, MD, USA. She is the NOAA Chief Scientist for satellite Global Positioning System radio occultation and currently works at the NOAA's Earth System Research Laboratory, Boulder, CO, USA, of the Office of Oceanic and Atmospheric Research.

Dr. Cucurull has won several national awards in recognition of her work, including the University Corporation for Atmospheric Research Outstanding Scientific and Technology Advancement Award (2007) and the NOAA David Johnson Award (2011).